Clinical Science (2017) **131** 1877–1893
DOI: 10.1042/CS20170271

PORTLAND PRESS

Research Article

FGF21 ameliorates diabetic cardiomyopathy by activating the AMPK-paraoxonase 1 signaling axis in mice

Fan Wu[1,*], Baile Wang[2,*], Saisai Zhang[3,*], Lihua Shi[3], Yanfang Wang[1], Rongrong Xiong[3], Xuebo Pan[3], Fanghua Gong[3], Xiaokun Li[1,3] and Zhuofeng Lin[3]

[1]College of Chinese Medicinal Materials, Jilin Agricultural University, Changchun, China; [2]State Key Laboratory of Pharmaceutical Biotechnology, The University of Hong Kong, Hong Kong; Department of Medicine, The University of Hong Kong, Hong Kong; [3]School of Pharmaceutical Sciences, Wenzhou Medical University, Wenzhou, China

Correspondence: Zhuofeng Lin (zhuofenglin@wzmc.edu.cn) or Xiaokun Li (xiaokunli@wzmc.edu.cn)

The aim of the present study is to explore the molecular mechanism of fibroblast growth factor 21 (FGF21) in protecting against diabetic cardiomyopathy (DCM). Streptozotocin/high-fat diet (STZ/HFD) was used to induced diabetes in FGF21-deficient mice and their wild-type littermates, followed by evaluation of the difference in DCM between the two genotypes. Primary cultured cardiomyocytes were also used to explore the potential molecular mechanism of FGF21 in the protection of high glucose (HG)-induced cardiomyocyte injury. STZ/HFD-induced cardiomyopathy was exacerbated in FGF21 knockout mice, which was accompanied by a significant reduction in cardiac AMP-activated protein kinase (AMPK) activity and paraoxonase 1 (PON1) expression. By contrast, adeno-associated virus (AAV)-mediated overexpression of FGF21 in STZ/HFD-induced diabetic mice significantly enhanced cardiac AMPK activity, PON1 expression and its biological activity, resulting in alleviated DCM. In cultured cardiomyocytes, treatment with recombinant mouse FGF21 (rmFGF21) counteracted HG-induced oxidative stress, mitochondrial dysfunction, and inflammatory responses, leading to increased AMPK activity and PON1 expression. However, these beneficial effects of FGF21 were markedly weakened by genetic blockage of AMPK or PON1. Furthermore, inactivation of AMPK also markedly blunted FGF21-induced PON1 expression but significantly increased HG-induced cytotoxicity in cardiomyocytes, the latter of which was largely reversed by adenovirus-mediated PON1 overexpression. These findings suggest that FGF21 ameliorates DCM in part by activation of the AMPK-PON1 axis.

Introduction

The prevalence of diabetes mellitus is growing rapidly. Amongst all the diabetic complications, cardiovascular disease is recognized as the primary cause of mortality in diabetic patients. Diabetic cardiomyopathy (DCM), a rare complication caused by diabetes and characterized by impaired cardiac structure and function, is not fatal but does inevitably progress to heart failure. A number of studies have indicated that DCM is considered to be associated with oxidative stress and mitochondrial dysfunction (which are regarded as the main incentives to initiate ventricular remodeling), and is characterized by fibrosis and heart dysfunction [1-3]. Therefore, the beneficial effects of attenuating diabetes-induced oxidative damage and the subsequent cardiac hypertrophy and fibrosis, are expected to prevent diabetes-induced cardiac injury and may be a potential therapeutic strategy for DCM.

Fibroblast growth factor 21 (FGF21), a novel hormone predominantly secreted by hepatic tissues, plays an important role in whole-body metabolic regulation during physiological and pathological conditions

*These authors contributed equally to this work.

Received: 31 March 2017
Revised: 20 May 2017
Accepted: 30 May 2017

Accepted Manuscript Online: 30 May 2017
Version of Record published: 7 July 2017

Clinical Science (2017) **131** 1877–1893
DOI: 10.1042/CS20170271

[4-7]. Mounting evidence from human studies indicates that several types of cardiovascular diseases including atherosclerosis, coronary heart disease, and myocardial infarction are associated with an elevated circulating FGF21 level [8,9]. Animal-based studies also demonstrate that FGF21 deficiency accelerates the development of these cardiovascular diseases in relevant animal models [10,11]. In ApoE-knockout mice, FGF21 ablation strongly accelerates the progression of atherosclerosis, and treatment with recombinant mouse FGF21 (rmFGF21) protein significantly attenuates atherosclerosis status [11]. Furthermore, FGF21 deficiency also accelerates isoproterenol- and ischemia–reperfusion-induced myocardial injury in mice [12-14], suggesting that FGF21 presents a cardiovascular protective effect in pathological status. Recently, our colleagues revealed that streptozotocin (STZ)-induced type 1 diabetic mice with FGF21 ablation were more susceptible to developing diabetic cardiomyopathy [15]. In addition, FGF21 deletion results in upregulated Nrf2-driven CD36 expression, exacerbated cardiac lipid uptake and accumulation, which in turn impairs cardiac lipid and glucose utilization, cardiac energy balance, as well as aggravates cardiac oxidative stress, and eventually accelerating the development of DCM [15]. However, the underlying mechanism by which FGF21 counteracts diabetes-induced myocardial injury remains enigmatic. In the present study, we use FGF21 KO mice and cellular experiments to explore the exact mechanism that FGF21 protects against DCM.

Methods

Animal models

FGF21 KO mice in C57BL/6J background were generated as previously described [16]. All the mice were housed in a room with controlled temperature ($23 \pm 1^{\circ}C$), a 12-h light-dark cycle, and had free access to water and diet. For the STZ-induced diabetic model, mice were first fed with a high-fat diet (HFD) for 4 weeks and then received intraperitoneal injection of a single dosage of STZ (Sigma–Aldrich, St. Louis, MO, dissolved in 0.1 M sodium citrate buffer, pH 4.5) at 100 mg/kg body weight, while age-matched control mice were fed with HFD accordingly and received a single injection of the same volume of sodium citrate buffer. Five days after the last injection of STZ, mice with hyperglycemia (3 h fasting blood glucose levels >250 mg/dl) were defined as diabetic as described previously [17]. When the diabetic models had been successfully induced, FGF21 KO male mice were also intravenously injected with 1×10^{12} viral particles of adeno-associated virus (AAV) encoding FGF21 or GFP. Glucose and insulin tolerance tests were performed as described previously [18]. All the animal studies were approved by the Animal Research Ethics Committee of Wenzhou Medical University.

Echocardiography and tissue Doppler imaging

Heart function was evaluated by transthoracic echocardiography (ECHO). ECHO was performed on mice using a Visual Sonics Vevo 2100 high-resolution imaging system (Visual Sonics, Toronto, ON, Canada) as described previously [19]. 2D and M-model images were obtained for measurements of systolic function [19], and diastolic function was assessed using pulsed-wave Doppler imaging as described in a previous study [20].

Biochemical and immunological assays

Plasma lipid profiles including total triglycerides, and total cholesterol levels were measured with commercial kits from Sigma (St. Louis, MO). Plasma levels of tumor necrosis factor α (TNF-α), interleukin-6 (IL-6), and monocyte chemoattractant protein 1 (MCP-1) were analyzed with immunoassays from R&D System Inc. (Minneapolis, MN). Serum insulin levels were tested with immunoassays from the Antibody and Immunoassay Services at the University of Hong Kong.

Histological analysis, cardiac superoxide, and apoptosis analysis

Cardiac sections were stained with hematoxylin-eosin (H&E) for morphological analysis or stained with dihydroethidium (DHE) to determine superoxide production in heart tissues [21], and stained with Sirius Red to reflect collagen accumulation [15]. Cardiac sections were also used to determine the apoptosis of cardiomyocytes using an *in situ* cell death detection assay (Roche, Mannheim, Germany). All slides were examined using an Olympus biological microscope BX41, and images were captured using Olympus DP72 color digital camera.

PON1 arylesterase activity and paraoxonase activity assay

Paraoxonase 1 (PON1) arylesterase activity and paraoxonase activity were determined as previously described [22,23]. In brief, PON1 arylesterase activity was spectrophotometrically measured using phenyl acetate as the substrate in 50-fold diluted serum (final) at 270 nm and 25°C. The assay mixture included stock buffer (500 mM phenyl acetate in methanol, 250-fold diluted) and reaction buffer (50 mM Tris/HCl, 1 mM $CaCl_2$, pH 8.0). The E_{270} for the reaction

is 1310 mol/l^{-1} · cm^{-1} and 1 unit of arylesterase activity is equal to 1 μmol of phenyl acetate hydrolyzed per ml per min.

Paraoxonase activity was measured spectrophotometrically at 412 nm using paraoxon as the substrate in 40-fold diluted serum (final) at 25°C. The assay mixture included stock buffer (400 mM phenyl paraoxon in methanol, 100-fold diluted) and reaction buffer (1.0 mM $CaCl_2$ in 0.05 M glycine buffer, pH 10.5, and no additional NaCl). An extinction coefficient (at 412 nm) of 16900 mol/l^{-1} · cm^{-1} was used for calculating units of paraoxonase activity, which is expressed as nanomoles of *p*-nitrophenol produced per min per ml of serum.

In vitro experiments on primary mouse cardiomyocytes

Cardiomyocytes were isolated from neonatal mice as described previously [24]. Cells were suspended in DMEM with 10% FBS (FBS-DMEM), seeded on to six-well plates, cultured overnight in FBS-DMEM with 5.6 mmol/l glucose, infected with adenovirus with dominant-negative (DN)-AMP-activated protein kinase (AMPK) for 24 h, and then replaced with FBS-DMEM with 33 mmol/l glucose (high glucose, HG) and rmFGF21 protein for various time points, as described in the figure legends. Intracellular reactive oxygen species (ROS) levels in mouse primary cardiomyocytes were determined by 5-(and-6)-chloromethyl-2′,7′-dichlorodihydrofluorescein diacetate (CM-H2DCFDA) or a fluorescent probe, as described in [25]. The fluorescence intensity (relative fluorescence units) was measured at an excitation and emission wavelength of 485 and 530 nm, respectively. Cardiomyocyte apoptosis was determined by flow cytometry.

Infection of recombinant adenovirus in cardiomyocytes

Recombinant adenovirus for the expression of a constitutively DN version of AMPKα was prepared as described previously [26]. Constitutively, DN-AMPKα carries a single mutation of the truncated form of the AMPK catalytic subunit α1 (Asp^{157} replaced by alanine). PON1 siRNA and a scramble control were designed and confirmed by our primary experiments, and the sequences were as follows: PON1 siRNA, 5′-TCTGCCTAGCATCAACGATAT-3′; β-klotho siRNA, 5′-UGCGCAAGGUCUCCGGUACUA-3′; and scramble, 5′-CATAGCCAATATATTTCCAGAT-3′. Recombinant adenovirus encoding GFP was used as the control. Primary mouse cardiomyocytes were infected with these adenoviruses at 50 p.f.u/cell for 36 h prior to HG or/and FGF21 treatment.

Isolation of mitochondria and measurement of mitochondrial respiratory chain complex activities

Mice were killed under deep anesthesia, and the cardiac tissues were immediately collected for cardiac mitochondria isolation using the procedures described previously [27]. Cultured cardiomyocytes in specific experiments were also collected for mitochondria isolation using the same methods. Measurement of mitochondrial respiratory chain (MRC) complex activities was performed using the same previously described methods [28].

Measurement of intracellular ROS

Intracellular ROS levels in mouse primary cardiomyocytes were determined using CM-H2DCFDA or a fluorescent probe as described in [28]. The fluorescence intensity (relative fluorescence units) was measured at an excitation and emission wavelength of 485 and 530 nm, respectively.

Immunoblotting and real-time PCR

Immunoblotting was performed as described previously [11]. The targetted proteins were probed with primary antibodies against phospho-AMPK (Thr^{192}), AMPK, phospho-acetyl-CoA carboxylase (ACC) (Ser^{79}), ACC, PON1, and GAPDH (Cell Signaling Technology Company). The protein bands were visualized with ECL reagents (GE Healthcare, Uppsala, Sweden) and quantitated using the NIH ImageJ software.

Real-time PCR was performed as described previously [11]. Simply, total RNA was extracted from cardiac tissues, and cDNA was synthesized by reverse transcription with random hexamer primers. Quantitative real-time PCR was performed using a SYBR Green QPCR system (Qiagen) with specific primers (Supplementary Table S1). The level of target gene expression was normalized against the *GAPDH* gene.

Statistical analysis

All data were expressed as mean ± S.E.M. Datasets were analyzed for statistical significance using the non-parametric Mann–Whitney U-test, Kruskal–Wallis, or two-way ANOVA analysis when specified. In all statistical comparisons, a P-value <0.05 was used to indicate a statistically significant difference.

Clinical Science (2017) 131 1877–1893
DOI: 10.1042/CS20170271

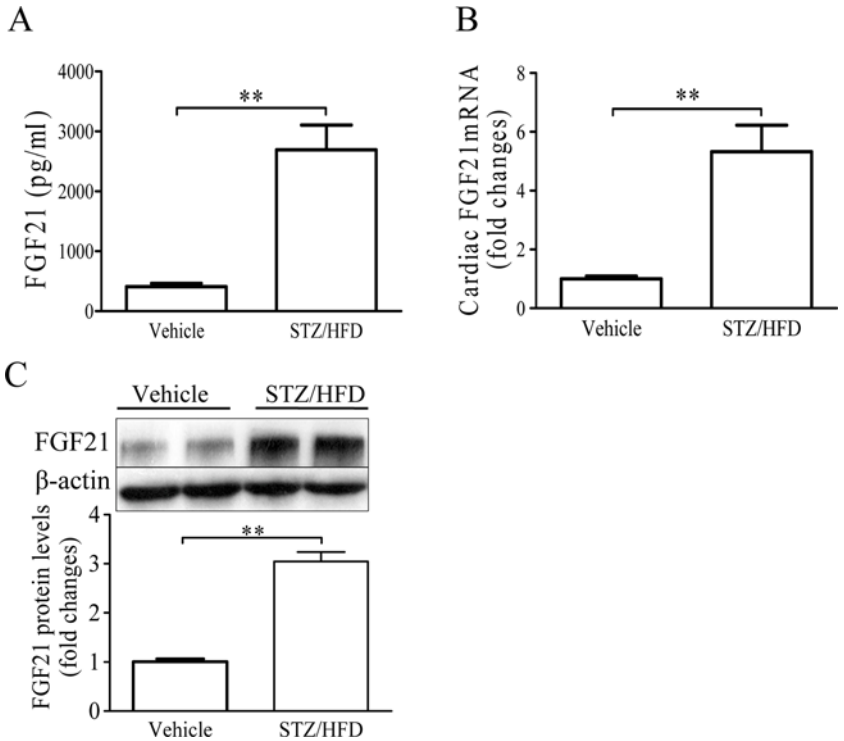

Figure 1. FGF21 expression is increased in STZ/HFD-induced diabetic mice

8-week-old male WT mice were treated as described in the *Methods* section, and killed at 16 weeks after STZ treatment. (**A**) Circulating FGF21 levels tested by ELISA. (**B**) Cardiac *FGF21* mRNA levels examined by real-time quantitative PCR. (**C**) Cardiac FGF21 protein levels determined by Western blot. $^{**}P<0.01$. $n=5$ for (A) and (B); $n=4$ for (C).

Results

FGF21 is increased in STZ/HFD-induced diabetic mice

To explore the relationship between FGF21 and DCM, 8-week-old male WT mice were used to generate a STZ/HFD-induced diabetic model as described in the *Methods* section. Different from the previous report [15], administration of STZ/HFD significantly increased serum FGF21 levels in WT mice (Figure 1A). Furthermore, cardiac *FGF21* mRNA and protein levels were also markedly elevated compared with the control group (Figure 1B,C), suggesting that elevated FGF21 in STZ/HFD-induced diabetic mice may be involved in the pathogenesis of DCM.

Loss of FGF21 accelerates cardiomyopathy in STZ/HFD-induced diabetic mice

To further explore the molecular mechanism of FGF21 in protecting against DCM, 8-week-old male FGF21 KO mice and age- and gender-matched WT littermate controls were used to generate a STZ/HFD-induced diabetic model as described in the *Methods* section. Consistent with the previous study [17], treatment with STZ/HFD significantly increased fed and fasting glucose levels, diminished glucose and insulin tolerance, as well as elevated total cholesterol and triglyceride concentrations in both FGF21 KO mice and WT controls. However, these effects were further augmented in FGF21 KO mice compared with those in WT mice (Supplementary Figure S1).

On the other hand, no significant difference in body weight was observed between KO and WT mice treated with STZ/HFD, whereas the ratio of heart weight to body weight in STZ/HFD-treated FGF21 KO mice was markedly increased as compared with STZ/HFD-treated WT controls (Figure 2A). Consistent with these results, histological analysis by H&E staining also revealed that FGF21 deficiency accelerated cardiomyocyte hypertrophy in STZ/HFD-induced diabetic mice compared with WT mice under the same treatment (Figure 2B). Furthermore, FGF21 deficiency also increased the expression of atrial natriuretic peptide (ANP) and angiotensinogen (ANG) in STZ/HFD-treated mice compared with the control group (Figure 2C), suggesting that the absence of FGF21 is related to cardiac hypertrophy in STZ/HFD-induced diabetic mice.

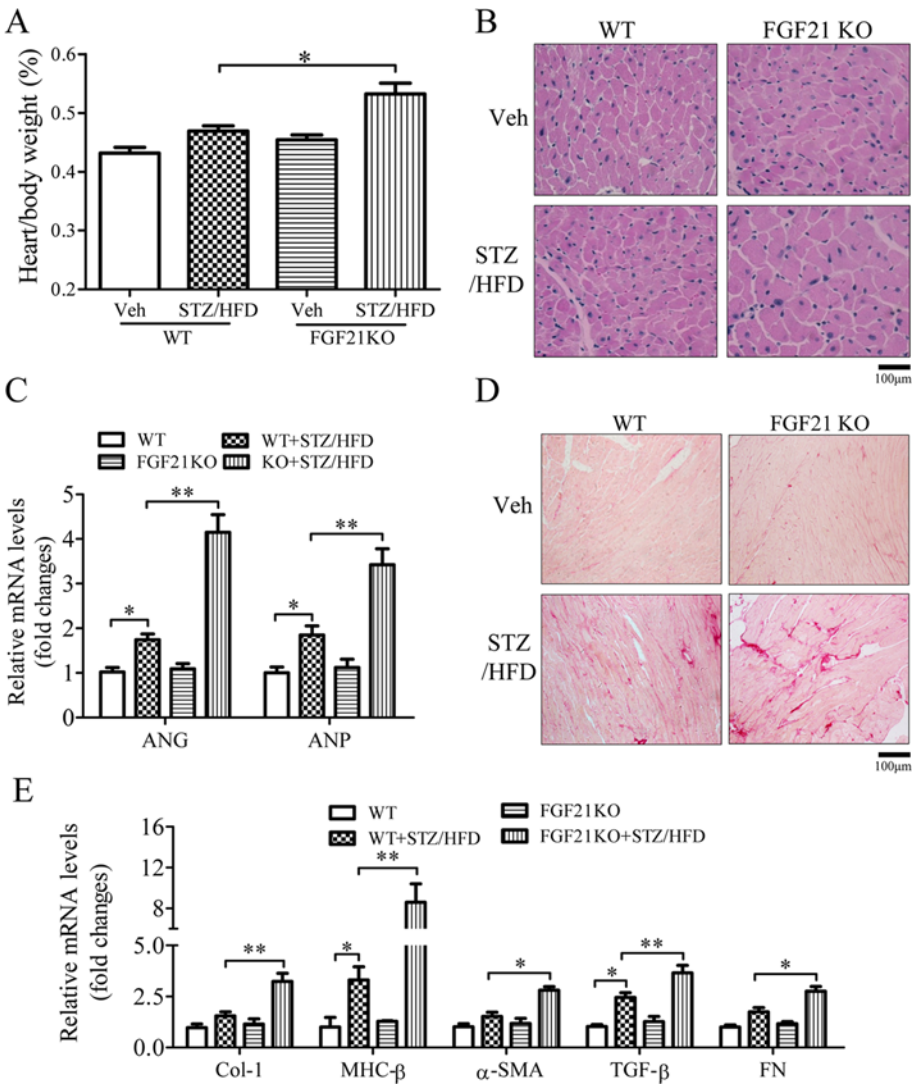

Figure 2. Loss of FGF21 accelerates hypertrophy and fibrosis in STZ/HFD-induced diabetic mice

8-week-old male FGF21 KO and age-matched WT littermates were treated as described in the *Methods* section, and killed at 16 weeks after STZ treatment. (**A**) Ratios of heart weight to body weight. (**B**) H&E staining of cardiac section (magnification ×200). (**C**) Cardiac mRNA expression levels of the hypertrophic markers ANG and ANP by real-time qPCR. (**D**) Sirius Red staining of cardiac section (magnification ×200). (**E**) Cardiac mRNA expression levels of fibrotic markers including collagen-1 (Col-1), MHC-β, α-smooth muscle actin (α-SMA), transforming growth factor β (TGF-β), and fibronectin (FN) tested by real-time qPCR. Data are presented as mean ± S.E.M. **P*<0.05; ***P*<0.01. *n*=6–7 in each group. NS, not significant.

In line with the histological change in cardiac tissues, we next explored the change in cardiac functions in STZ/HFD-induced diabetic mice. As expected, FGF21 deficiency further accelerated cardiac dysfunction in STZ/HFD-treated diabetic mice, as evidenced by increased LV end-diastolic and -systolic diameters, LV end-diastolic and -systolic volumes, and decreased ejection fraction (Table 1), compared with those in WT mice under the same treatment. On the other hand, tissue and pulse Doppler imaging analysis indicated that FGF21 deficiency decreased E-wave velocity and increased A-wave velocity as well as the E/E′ ratio in STZ/HFD-induced mice compared with WT controls (Table 2), suggesting that FGF21 deficiency accelerated diastolic dysfunction in STZ/HFD-treated mice. Taken together, these data indicated that FGF21 deficiency could increase the susceptibility for the pathogenesis of DCM in mice.

As cardiac fibrosis is one of the most important pathogenic routes of DCM, we measured cardiac collagen accumulation between FGF21 KO and WT controls. The results of Sirius Red staining indicated that FGF21 deficiency

Clinical Science (2017) **131** 1877–1893
DOI: 10.1042/CS20170271

Table 1 FGF21 deficiency exacerbates diabetes-induced systolic dysfunction

Variants	WT + vehicle (*n*=6)	WT + STZ/HFD (*n*=7)	KO + vehicle (*n*=6)	KO + STZ/HFD (*n*=7)
LVID; d (mm)	3.47 ± 0.03	3.76 ± 0.06	3.50 ± 0.09	4.02 ± 0.13†‡
LVID; s (mm)	1.96 ± 0.07	2.36 ± 0.09*	1.99 ± 0.03	2.61 ± 0.13†‡
LV vol; d (μl)	56.21 ± 1.32	58.13 ± 2.15	57.06 ± 4.13	62.13 ± 4.15†‡
LV vol; s (μl)	10.12 ± 0.36	16.30 ± 1.29*	10.92 ± 0.45	23.43 ± 2.06†‡
EF (%)	82.62 ± 1.82	74.31 ± 2.13*	81.91 ± 2.32	63.75 ± 3.15†‡
FS%	43.52 ± 1.35	38.23 ± 2.26*	42.90 ± 2.53	31.79 ± 2.17†‡
LV mass (mg)	86.13 ± 4.79	98.75 ± 3.15*	101.72 ± 3.21	129.1 ± 4.62†‡
HR	641 ± 32	639 ± 27	645 ± 35	641 ± 30

8-week-old male FGF21 KO and age-matched WT littermates were treated as described in the *Methods* section, heart functions were evaluated by transthoracic ECHO before being killed at 16 weeks post-treatment with STZ. Data are presented as mean ± S.D. Abbreviations: EF, ejection fraction; FS, fractional shortening; HR, heart rate under conscious condition; LV vol; d, LV end-diastolic volume; LV vol; s, LV end-systolic volume; LVID; d, LV end-diastolic diameter; LVID; s, LV end-systolic diameter*$P<0.05$ compared with WT + vehicle; †, $P<0.05$ compared with KO + vehicle. ‡, $P<0.05$ compared with WT + STZ/HFD.

Table 2 FGF21 deletion accelerated diabetes-induced diastolic dysfunction

Variants	WT + vehicle (*n*=5)	WT + STZ/HFD (*n*=5)	KO + vehicle (*n*=5)	KO + STZ/HFD (*n*=5)
E-wave, mm/s	693 ± 32.1	584 ± 25.3*	675 ± 35.6	552 ± 27.8†
A-wave, mm/s	453 ± 25.7	402 ± 23.4	437 ± 23.2	453 ± 20.2
E/A ratio	1.52 ± 0.03	1.46 ± 0.07	1.53 ± 0.05	1.22 ± 0.04†‡
IVRT, ms	13.8 ± 3.1	18.2 ± 3.3*	14.6 ± 2.7	21.5 ± 2.9†‡
DT, ms	21.3 ± 1.8	26.5 ± 2.5*	20.6 ± 2.0	29.6 ± 3.1†‡
E′, mm/s	30.7 ± 3.6	23.5 ± 1.8*	29.3 ± 3.0	20.8 ± 2.6†‡
E/E′ ratio	22.6 ± 0.08	24.8 ± 0.05*	23.0 ± 0.07	26.6 ± 0.09†‡

8-week-old male FGF21 KO and age-matched WT littermates were treated as described in the *Methods* section, diastolic functions were evaluated by tissue and plus Doppler models. Data are presented as means ± S.E.M. Abbreviations: A-wave, mitral Doppler A velocity; DT, deceleration time; E-wave, peak early transmitral inflow mitral E velocity; E′, early diastolic tissue Doppler velocity; IVRT, isovolumetric relaxation time. *, $P<0.05$ compared with WT + vehicle, †, $P<0.05$ compared with KO + vehicle. ‡, $P<0.05$ compared with WT + STZ/HFD.

distinctly increased cardiac fibrosis and collagen accumulation in STZ/HFD-treated mice (Figure 2D). In line with these results, gene expression analysis also demonstrated that cardiac mRNA expression levels of collagen-related genes including Col-1, MHC-β, α-smooth muscle actin (α-SMA), and transforming growth factor β (TGF-β) as well as fibrosis-related genes fibronectin (FN) were markedly upregulated in STZ/HFD-treated FGF21 KO mice, compared with those in WT mice with the same administration (Figure 2E), suggesting that FGF21 deficiency accelerates cardiac fibrosis in diabetic mice.

FGF21 deficiency exacerbates cardiac oxidative stress, mitochondria dysfunction, apoptosis, and inflammation in STZ/HFD-induced diabetic mice

Compelling evidence demonstrates that the development of DCM is related to the induction of cardiac oxidative stress, as characterized by the production of ROS, leading to mitochondrial dysfunction, which in turn promotes cardiac oxidative stress [29,30]. Therefore, we investigated the effect of FGF21 deletion on the production of ROS and mitochondrial dysfunction in STZ/HFD-induced diabetic mice. As expected, cardiac ROS levels detected by DHE staining (Supplementary Figure S2A,B) and the percentage of apoptotic cardiomyocytes determined by TUNEL (Supplementary Figure S2C,D) were significantly higher in STZ/HFD-treated FGF21 KO mice than those in WT controls. Furthermore, a significant attenuation in the activities of MRC complexes I and V, but not complexes II + III and IV, was observed in STZ/HFD-treated WT mice, and these effects were further augmented in STZ/HFD-treated FGF21 KO mice (Supplementary Figure S2E).

Considering that a pro-inflammatory status is often associated with the development of cardiac hypertrophy, we also investigated the effects of FGF21 absence on cardiac and systemic inflammation. Our results indicated that the mRNA levels of several inflammatory cytokines including TNF-α, IL-6, and MCP-1 were increased in

Clinical Science (2017) **131** 1877–1893
DOI: 10.1042/CS20170271

Table 3 AAV-mediated FGF21 expression blocks diabetes-induced cardiac dysfunction

Variants	KO + STD (*n*=6)	KO + STZ/HFD AAV-GFP (*n*=6)	KO + STZ/HFD AAV-FGF21 (*n*=6)
LVID; d (mm)	3.52 ± 0.07	4.06 ± 0.03**	4.02 ± 0.02
LVID; s (mm)	1.97 ± 0.02	2.76 ± 0.05**	2.43 ± 0.07†
LV vol; d (μl)	57.32 ± 1.32	61.72 ± 3.43	58.65 ± 1.75
LV vol; s (μl)	10.27 ± 0.41	23.21 ± 1.32**	13.72 ± 0.52†
EF (%)	82.21 ± 2.62	62.32 ± 2.15*	78.91 ± 4.37†
FS (%)	42.03 ± 1.62	32.02 ± 2.13*	39.56 ± 2.15†
LV mass (mg)	85.7 ± 4.33	137.2 ± 4.52**	111.6 ± 4.21†
HR (bmp)	638 ± 37	641 ± 33	640 ± 29

8-week-old FGF21 KO male mice were induced successfully to a diabetes model as described in the *Methods* section, and then intravenously injected with 1×10^{12} viral particles of AAV encoding FGF21 or GFP. Heart functions were evaluated by transthoracic ECHO before being killed at 16 weeks post-treatment with AAV-FGF21 or GFP. Eight-week-old FGF21 KO male mice with a chow diet were used as a control. Data are presented as mean ± S.D. Abbreviations: EF, ejection fraction; FS, fractional shortening; HR, heart rate; LV vol; d, LV end-diastolic volume; LV vol; s, LV end-systolic volume; LVID; d, LV end-diastolic diameter; LVID; s, LV end-systolic diameter. *, $P<0.05$ compared with KO + STD; ** $P<0.05$ compared with KO + STD; †, $P<0.05$ compared with AAV-GFP.

Table 4 Overexpression of FGF21 attenuates diabetes-induced diastolic dysfunction

Variants	KO + STD (*n*=5)	KO + STZ/HFD AAV-GFP (*n*=5)	KO + STZ/HFD AAV-FGF21 (*n*=5)
E-wave, mm/s	635 ± 19.3	531 ± 22.1*	595 ± 18.6†
A-wave, mm/s	421 ± 31.7	356 ± 37.3	407 ± 31.9
E/A ratio	1.51 ± 0.09	1.49 ± 0.1	1.46 ± 0.12
IVRT, ms	13.8 ± 2.2	20.3 ± 2.6*	15.6 ± 2.1†
DT, ms	20.3 ± 2.0	28.2 ± 1.9*	23.6 ± 2.3†
E′, mm/s	29.0 ± 2.7	19.5 ± 1.7*	25.3 ± 3.2†
E/E′	21.9 ± 0.7	27.2 ± 1.2*	23.5 ± 1.3†

8-week-old FGF21 KO male mice were induced successfully to a diabetes model as described in the *Methods* section, and then intravenously injected with 1×10^{12} viral particles of AAV encoding FGF21 or GFP. Diastolic functions were evaluated by tissue and plus Doppler models. Data are presented as means ± S.E.M. Abbreviations: A-wave, mitral Doppler A velocity; DT, deceleration time; E-wave, peak early transmitral inflow mitral E velocity; E′, early diastolic tissue Doppler velocity; IVRT, isovolumetric relaxation time. *, $P<0.05$ compared with KO + STD group; †, $P<0.05$ compared with AAV-GFP group.

STZ/HFD-treated WT mice accompanied by cardiac hypertrophy. Interestingly, these inductions were further worsened in STZ/HFD-treated FGF21 KO mice (Supplementary Figure S2F). Furthermore, a similar pattern was also observed in the serum levels of these inflammatory factors (Supplementary Figure S2G).

Overexpression of FGF21 improves DCM via attenuation of cardiac hypertrophy, fibrosis, oxidative stress, and cardiac inflammation in mice

To further investigate the role of FGF21 in DCM, 8-week-old FGF21 KO male mice were induced to a diabetic model, and then infected with AAV encoding mouse FGF21 or GFP, respectively. As expected, AAV-mediated FGF21 overexpression significantly elevated the circulating FGF21 level (Supplementary Figure S3A), ameliorated diabetes status, as evidenced by decreased fed and fasting glucose levels, as well as improviedglucose and insulin tolerance compared with AAV-GFP controls (Supplementary Figure S3B–E). In- ine with these results, we next examined the changes in cardiac function after treatment with AAV-FGF21. Consistent with the improvement of diabetic profiles, AAV-mediated overexpression of FGF21 significantly improved systolic dysfunction in STZ/HFD-induced diabetic mice, shown as decreased LV end-diastolic and -systolic diameters, LV end-diastolic and -systolic volumes, and increased ejection fraction (Table 3). In addition, overexpression of FGF21 also reversed diastolic dysfunction in STZ/HFD-induced diabetic mice (Table 4). Taken together, these data demonstrated that FGF21 could markedly improve cardiac dysfunction in STZ/HFD-induced diabetic mice.

On the other hand, AAV-mediated overexpression of FGF21 dramatically attenuated cardiac collagen accumulation and fibrosis in STZ/HFD-induced diabetic mice as determined by H&E or Sirius Red staining respectively (Figure 3A), and markedly decreased cardiac mRNA levels of collagen- and fibrosis-related genes including Col-1, MHC-β, α-SMA, TGF-β, and FN (Figure 3B). Furthermore, treatment with AAV-FGF21 also reversed the elevated cardiac

PORTLAND PRESS

Clinical Science (2017) **131** 1877–1893
DOI: 10.1042/CS20170271

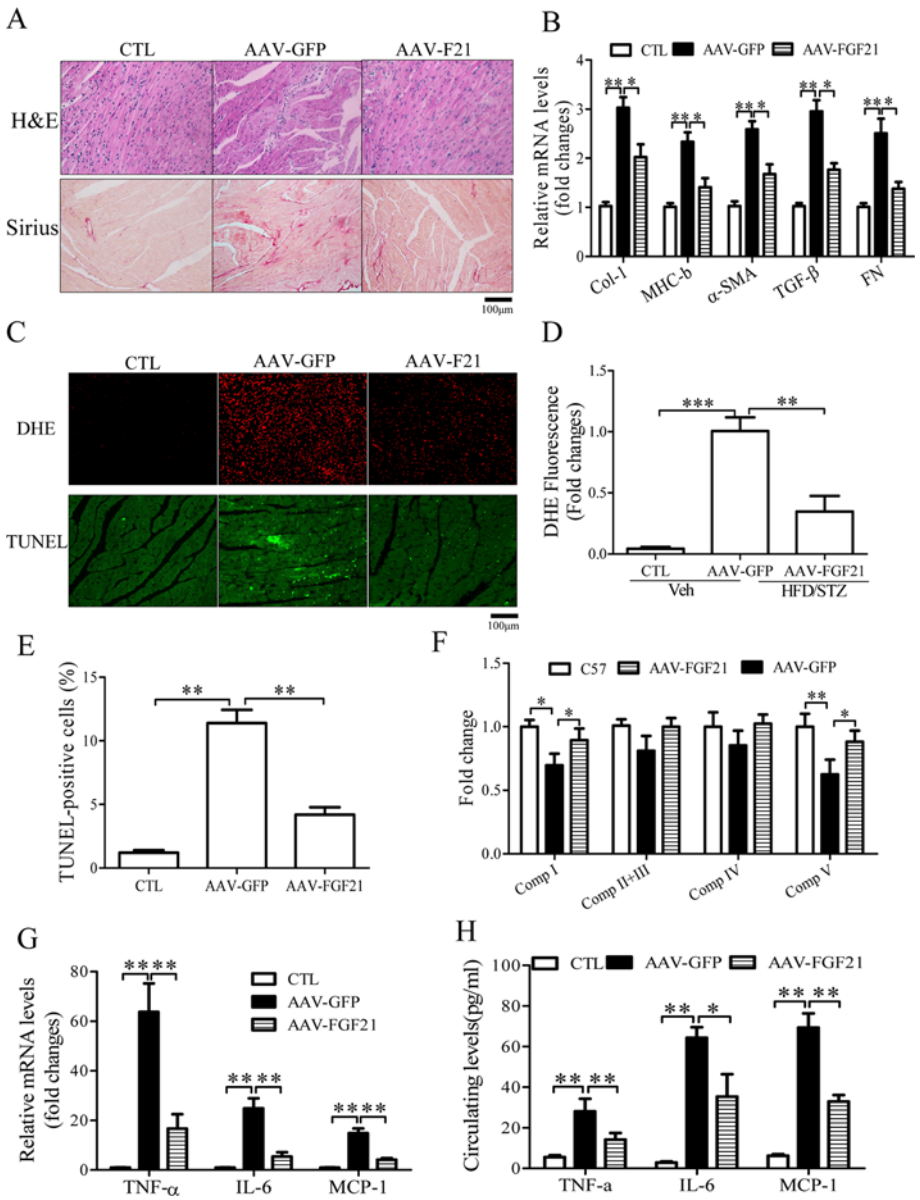

Figure 3. AAV-mediated overexpression of FGF21 attenuates cardiac fibrosis, oxidative stress and mitochondrial dysfunction, and inhibits local and systemic inflammation in mice

8-week-old FGF21 KO male mice were induced successfully to a diabetes models, and then intravenously injected with 1×10^{12} viral particles of AAV encoding FGF21 or GFP. Eight-week-old FGF21 KO male mice with a standard chow diet were used as control. All mice were killed 16 weeks after treatment with AAV-FGF21 or GFP. (**A**) Cardiac H&E and Sirius Red staining (magnification ×200). (**B**) Cardiac mRNA levels of fibrosis factors including Col-1, MHC-β, α-SMA, TGF-β, and FN. (**C**) Representative imaging of DHE and TUNEL staining for intracellular ROS levels and cardiomyocyte apoptosis, respectively (magnification ×200). (**D**) Intracellular ROS levels tested by DHE staining. (**E**) Cardiomyocyte apoptosis levels examined by TUNEL. (**F**) The activities of MRC complexes of cardiac tissues. (**G**) Cardiac mRNA levels of local inflammatory factors including TNF-α, IL-6, and MCP-1. (**H**) Circulating levels of inflammatory factors including TNF-α, IL-6, and MCP-1. Data are presented as mean ± S.E.M. *P<0.05; ** P<0.01. n=6 in each group.

ROS content (Figure 3C,D) and cardiomyocyte apoptosis (Figure 3C,E), improved the reduction in MRC complex I and V activities (Figure 3F), and inhibited cardiac mRNA levels of inflammatory genes including TNF-α, IL-6, and MCP-1 (Figure 3G) as well as their circulating levels (Figure 3H).

Clinical Science (2017) **131** 1877–1893
DOI: 10.1042/CS20170271

β-klotho is obligatory for FGF21 protection against HG-induced oxidative stress and inflammation in primary mouse cardiomyocytes

Previous studies have demonstrated that β-klotho is indispensable for FGF21 bioactivity [31]. To investigate the role of β-klotho in FGF21 protection against DCM, we first examined the expression of β-klotho in cardiac tissues of STZ/HFD-induced diabetic mice and control mice. Interestingly, a significant upregulation of β-klotho expression was observed in STZ/HFD-treated WT mice compared with the controls (Supplementary Figure S4A). To investigate whether HG affects the expression of β-klotho in cardiomyocytes, primary mouse cardiomyocytes were directly exposed to HG (33 mmol/l). Surprisingly, incubation of primary cardiomyocytes with HG led to a progressive increase in β-klotho (Supplementary Figure S4B) accompanied by a time-dependent increase in intracellular ROS production (Supplementary Figure S4C).

To further explore the role of β-klotho in FGF21 protection against DCM, primary cardiomyocytes were infected with adenovirus encoding siRNA-β-klotho before treatment with HG and FGF21. As expected, treatment with rm-FGF21 in primary cardiomyocytes significantly restored HG-induced elevated intracellular ROS content and mRNA levels of TGF-β, IL-6, and FN (Supplementary Figure S4D–H). However, these protective effects of FGF21 against HG-induced cytotoxicity were strongly abrogated by siRNA-mediated knockdown of β-klotho (Supplementary Figure S4D–H), suggesting that β-klotho is indispensable for FGF21 protection against HG-induced cardiomyocyte injury.

FGF21 alleviates HG-induced oxidative stress and fibrosis by activating the AMPK signaling pathway

Previous studies have demonstrated that AMPK, a major cellular sensor of energy availability, is involved in the progression of cardiac injury caused by different factors [32-34]. To explore whether AMPK is involved in FGF21 against diabetes-induced cardiac injury, we first evaluated AMPK activity in FGF21 KO and WT mice. Immunoblotting analysis demonstrated that the phosphorylation level of AMPK and its downstream target ACC were significantly decreased in STZ/HFD-induced diabetic mice, compared with those in the controls. Furthermore, FGF21 deficiency further accelerated the decrease in cardiac p-AMPK and p-ACC levels in STZ/HFD-induced diabetic mice (Figure 4A,B). By contrast, treatment with AAV-FGF21 markedly reversed the reduction in cardiac p-AMPK and p-ACC levels in STZ/HFD-treated mice (Figure 4C,D), suggesting that the protective effect of FGF21 against diabetes-induced cardiac injury is related to AMPK activity in mice.

To further determine the role of AMPK in FGF21 against diabetes-induced cardiac injury, we examined the direct effect of AMPK in FGF21 protection against HG-induced cardiomyocyte injury. As expected, incubation of primary mouse cardiomyocytes with HG significantly decreased p-AMPK levels (Figure 5A), accompanied by a drastic increase in intracellular ROS accumulation and cardiomyocyte apoptosis, an obvious decrease in MRC complex I and V activities, as well as a marked elevation of mRNA expression levels of TGF-β, FN, and ANP (Figure 5B–E). Interestingly, these HG-induced effects were markedly abrogated by treatment with rmFGF21 (Figure 5B–E). However, these protective effects of FGF21 against HG-induced cardiomyocyte injury were markedly blunted by genetic inhibition of AMPK activities with infection of adenovirus-mediated DN AMPK (Figure 5B–E), suggesting that AMPK plays an indispensable role in FGF21 protection against HG-induced cardiomyocyte injury.

PON1 mediates the protective effect of FGF21 against HG-induced oxidative stress, mitochondrial dysfunction, and inflammatory response in cardiomyocytes

PON1, a member of the paraoxonase subfamily, is involved in the onset and development of cardiovascular diseases [35-37]. To explore whether PON1 participates in FGF21 protection against DCM, we first tested the expression of PON1 in both STZ/HFD-treated FGF21 KO and WT mice. As expected, the cardiac PON1 protein and its mRNA levels, as well as arylesterase activity and PON1 activity, were significantly decreased in STZ/HFD-treated WT, and these effects were further down-regulated in STZ/HFD-treated FGF21 KO mice (Figure 6A–D). Intriguingly, treatment with AAV-FGF21 markedly reversed the reduction in cardiac PON1 expression as well as its arylesterase and paraoxonase activities in STZ/HFD-treated mice (Figure 6E–H), suggesting that PON1 may play a pivotal role in FGF21 protection against DCM.

To further determine the role of PON1 in FGF21 against DCM, we next tested the direct effect of PON1 in FGF21 protection against HG-induced cardiomyocyte injury. In line with our previous observations in mice, incubation of primary mouse cardiomyocytes with FGF21 significantly enhanced PON1 expression in a dosage-

Clinical Science (2017) **131** 1877–1893
DOI: 10.1042/CS20170271

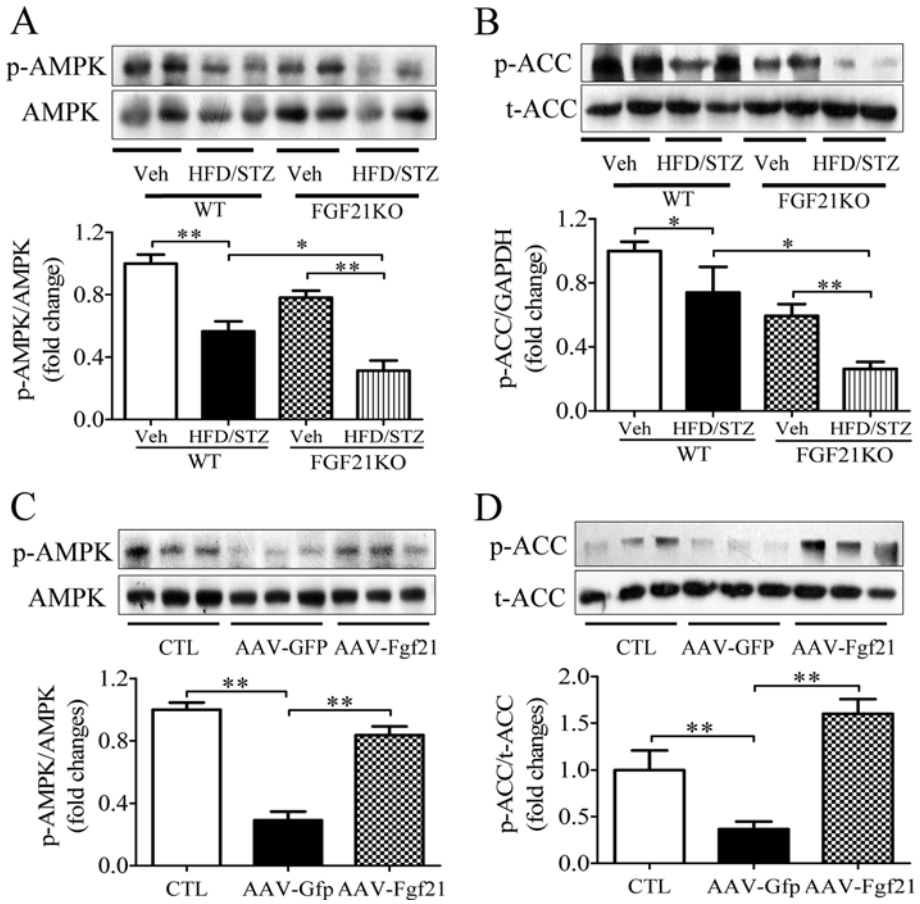

Figure 4. Cardiac AMPK activities are decreased in STZ/HFD-induced diabetic mice

Immunoblot analysis for expression levels of p-AMPK/total-AMPK (**A**,**C**) and ACC/phospho-ACC (**B**,**D**), in cardiac tissues collected in Figure 2 and Figure 3, respectively.

and time-dependent manner (Figure 7A,B). However, treatment of primary cardiomyocytes with FGF21 reversed HG-elevated intracellular ROS accumulation, decreased MRC complex I and V activities, upregulated mRNA levels of TGF-β, FN, and IL-6, and these FGF21-induced effects were strongly blunted by genetic inhibition of PON1 with siRNA (Figure 7C–F), suggesting that PON1 may at least, in part, mediate the protective effect of FGF21 against HG-induced cardiomyocyte injury.

FGF21 alleviates HG-induced cytotoxicity by activating the AMPK-dependent PON1 signal in cardiomyocytes

Based on our results that FGF21 alleviated HG-induced oxidative stress and fibrosis by activating the AMPK signaling pathway, we further explored whether AMPK is involved in the regulation of FGF21-induced PON1 expression in cardiomyocytes. As expected, FGF21-induced PON1 expression was strongly blunted by infection with adenovirus-mediated expression of DN AMPK (Figure 8A), which was accompanied by an increased intracellular ROS accumulation, upregulated the expression of TGF-β, FN, and IL-6, as well as inhibited MRC complex I and V activities (Figure 8B–E). Interestingly, these effects were strongly reversed when infected with adenovirus-PON1 (Figure 8B–E). Taken together, these data demonstrate that FGF21-induced PON1 expression is mediated by the AMPK signal pathway, and PON1 mediates the protective effect of FGF21 against HG-induced cytotoxicity in cardiomyocytes independently.

Discussion

Diabetes is currently a serious global issue. Amongst all the complications of diabetes, DCM is considered to be the primary cause of mortality in diabetic patients. A recent study involving STZ-induced type 1 diabetic mice indicated

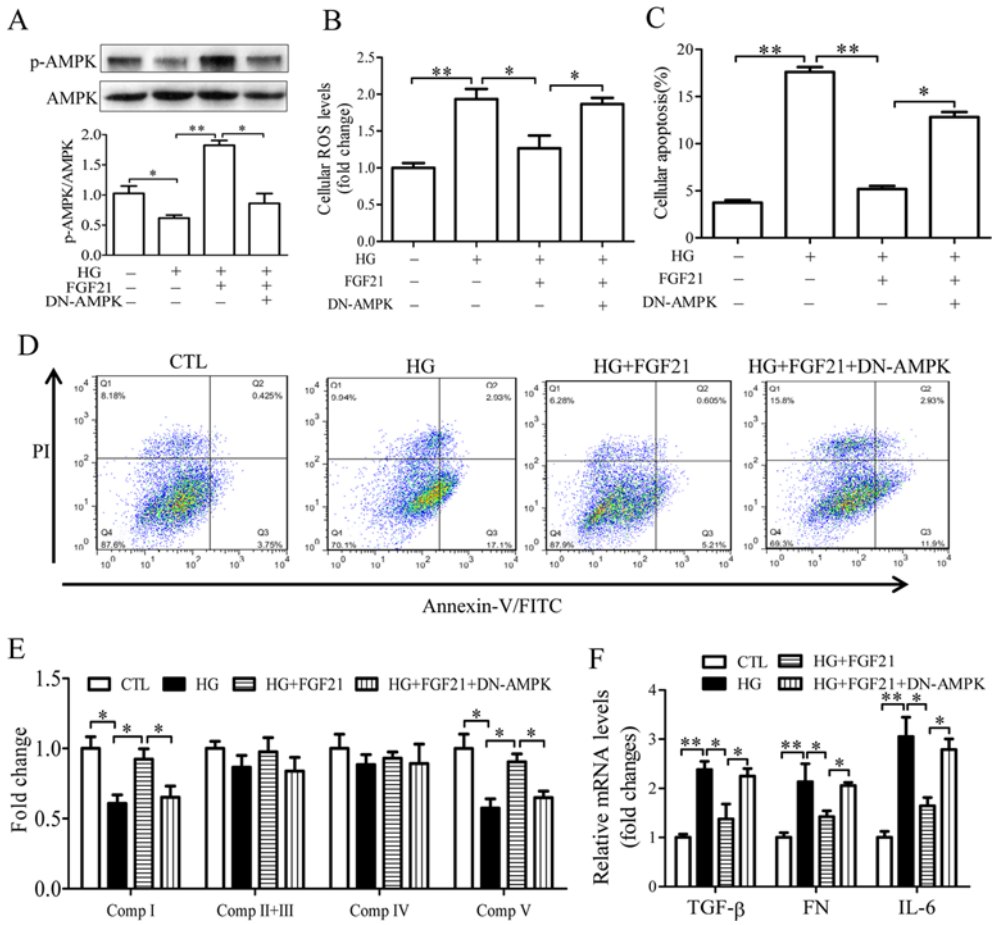

Figure 5. AMPK mediates the protective effects of FGF21 against HG-induced oxidative stress and mitochondrial dysfunction in cardiomyocytes

Primary mouse cardiomyocytes isolated from C57BL/6J mice were infected with adenovirus with DN AMPK and PON1 for 36 h, then incubated with HG (33 mM) for 6 h, followed by treatment with rmFGF21 (50 ng/ml) or vehicle for 24 h. (**A**) Immunoblot analysis for p-AMPK, total AMPK after 24 h of FGF21 treatment. (**B**) Cellular ROS levels measured by DCFH-DA assay. (**C**) Results of cardiomyocyte apoptosis measured by flow cytometry. (**D**) Representative plot of cellular apoptosis measured by flow cytometry. (**E**) The activities of MRC complex measured at 24 h after treatment. (**F**) The mRNA expression levels of TGF-β, FN, and IL-6. Data are presented as mean ± S.E.M. $^{*}P<0.05$, $^{**}P<0.01$. All *in vitro* data were obtained from at least four independent experiments.

that FGF21 deficiency rendered mice more susceptible to develop DCM [15]. However, the exact mechanism of FGF21 protection against DCM is still obscure. The present study demonstrates that FGF21 deficiency lessens AMPK activation and PON1 expression and promotes cardiac injury in STZ/HFD-induced diabetic mice. Overexpression of FGF21 significantly increases AMPK activation and PON1 content in mice, accompanied by improvement of cardiac injury. Furthermore, treatment with FGF21 reverses HG-induced oxidative stress, mitochondrial dysfunction, and inflammatory response by activating the AMPK-PON1 axis in primary cardiomyocytes. Taken together, these data demonstrate that the FGF21-AMPK-PON1 axis couples the protective effects of FGF21 in the protection of DCM in mice.

FGF21, a member of the endocrine FGF subfamily, is a metabolic hormone with pleiotropic effects on glucose and lipid metabolism and insulin sensitivity. Animal-based studies demonstrate that FGF21 lowers glucose and triglyceride levels, and exhibits insulin-sensitizing properties in diabetic rodents and monkeys [6,38]. A recent study indicated that loss of FGF21 worsened DCM in STZ-induced type 1 diabetic mice [15]. In line with this observation, we also found that FGF21 deficiency accelerated cardiomyopathy accompanied by ameliorated cardiac hypertrophy (Figure 2), elevated cardiac oxidative stress, improved mitochondrial dysfunction (Figure 3), and enhanced inflammation and fibrosis (Figure 4) in STZ/HFD-induced diabetic mice. On the other hand, we also found that overexpression

Clinical Science (2017) **131** 1877–1893
DOI: 10.1042/CS20170271

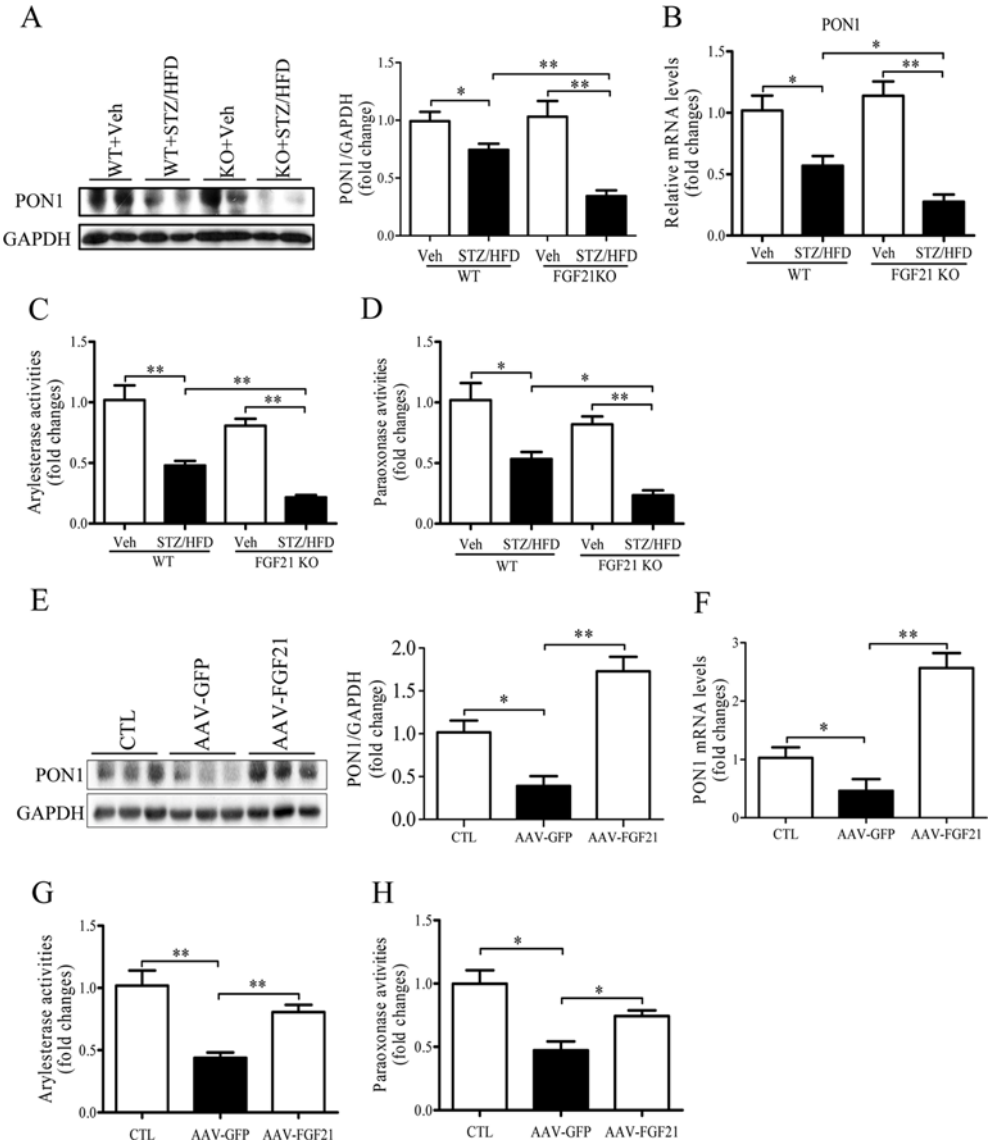

Figure 6. FGF21 deletion decreased cardiac PON1 expressional levels and blood paraoxonase activity in STZ/HFD-induced diabetic mice

Cardiac tissues and serum samples collected in Figure 2 and Figure 3 were used to test the expressional levels of PON1. (**A**,**E**) Cardiac PON1 levels tested by immunoblot analysis. (**B**,**F**) Cardiac *PON1* mRNA levels examined by real-time quantitative PCR. (**C**,**G**) Serum arylesterase activities and (**D**,**H**) paraoxonase activities in STZ/HFD-induced diabetic mice. Data are presented as mean ± S.E.M. $^{*}P<0.05$, $^{**}P<0.01$; n=6–7 in mice.

of FGF21 significantly attenuates DCM, followed by decreased cardiac oxidative stress, enhanced MRC complex activities, and inhibited inflammation and fibrosis in STZ/HFD-induced diabetic mice (Figure 5). Taken together, these data indicate that FGF21 protection against DCM may be related to improved mitochondrial function. To support this, FGF21 has been reported to regulate mitochondrial function by activating the AMPK-Sirt1-PGC1α pathway [39].

Klotho, a transmembrane protein, provides some control over the sensitivity of an organism to insulin and appears to be involved in ageing [40]. Recently, β-klotho, a member of the klotho family, was found to physically interact with FGF receptors 1c and 4, thereby increasing the ability of these FGF receptors to bind with FGF21 and activate the downstream signaling pathway [41]. Knockdown of β-klotho by siRNA in adipocytes diminishes glucose uptake induced by FGF21 [41]. These findings indicate that β-klotho plays an indispensable role in the FGF21-mediated

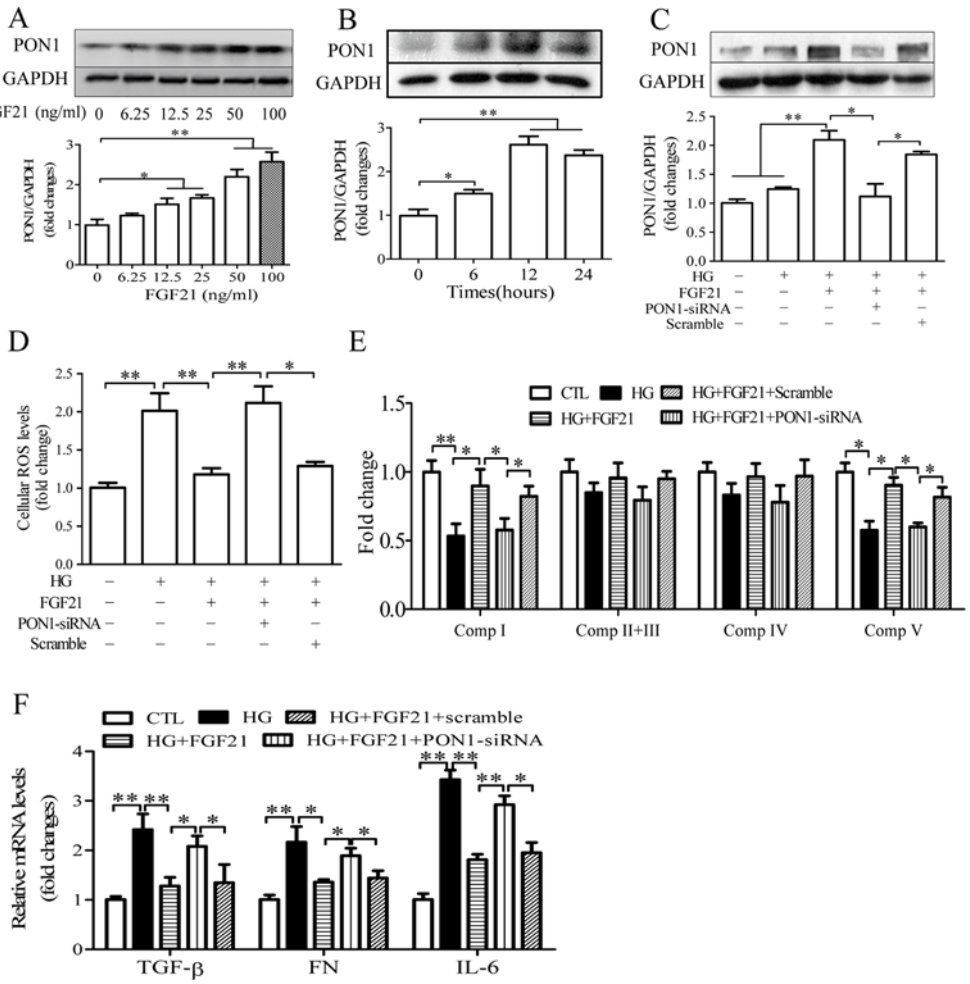

Figure 7. The effects of FGF21 on protection against HG-induced cytotoxicity are abrogated by genetic inhibition of PON1 in cardiomyocytes

(**A**,**B**) Primary mouse cardiomyocytes were treated with an increasing concentration of rmFGF21 (6.25–100 ng/ml) for 24 h or with a 50 ng/ml dosage of rmFGF21 at different time points (6–24 h), PON1 expression was measured by immunoblot analysis. (**C**–**F**) Primary mouse cardiomyocytes were infected with adenovirus expressing PON1-siRNA or a scramble for 36 h, followed by treatment with HG (33 mM) and/or rmFGF21 (50 ng/ml) for various periods. (C) Immunoblot analysis for PON1 expression. (D) Intracellular ROS levels measured by DCFH-DA assay. (E) The activities of MRC complex 6 h after treatment. (F) Cellular mRNA levels of TGF-β, FN, and IL-6 tested by real-time qPCR. Data are presented as mean ± S.E.M. $^{*}P<0.05$, $^{**}P<0.01$. All *in vitro* data were obtained from at least four independent experiments.

maintenance of glucose hemostasis and pathogenesis of diabetes. In the present study, different from a previous report that β-klotho expression in pancreatic islets was significantly attenuated when directly treated with HG [42], cardiac β-klotho expression was significantly upregulated in STZ/HFD-treated WT mice, and this elevated profile was markedly abrogated in FGF21-deficient mice under the same status, suggesting that FGF21 deficiency may affect cardiac expression of β-klotho in mice. Furthermore, our *in vitro* data also indicated that genetic inhibition of β-klotho by RNA interference almost reversed the protective effects of FGF21 against HG-induced oxidative stress and mitochondrial dysfunction, suggesting that β-klotho is essential for FGF21 protection against diabetes-induced cardiac injury.

Mounting evidence indicates that DCM is closely associated with increased oxidative stress and mitochondrial dysfunction. Under physiological conditions, ROS production by cardiomyocytes is regulated by a number of enzymes and antioxidants, and there is a physiological balance between ROS and antioxidants. However, under pathological conditions, such as diabetes, this balance is disrupted by hyperglycemia followed by overproduction of ROS, and then initiates harmful effects on cardiomyocytes, resulting in mitochondrial dysfunction, myocardial cell death, subsequent hypertrophy and fibrosis, and eventually leads to cardiac dysfunction [3]. PON1 was first discovered through

Clinical Science (2017) **131** 1877–1893
DOI: 10.1042/CS20170271

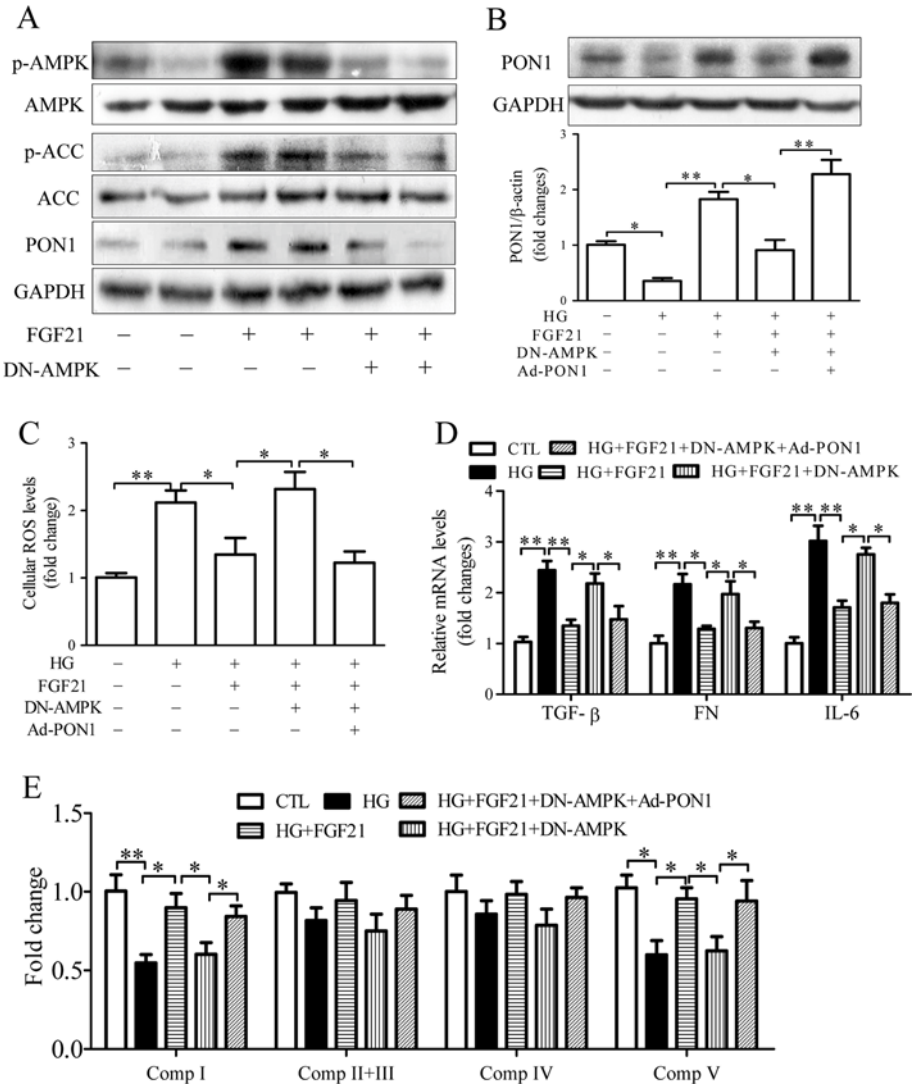

Figure 8. AMPK-dependent PON1 activity is essential for the protective effect of FGF21 against HG-induced cytotoxicity in cardiomyocytes

Primary mouse cardiomyocytes were infected with adenovirus with DN AMPK and PON1 for 36 h, then incubated with HG (33 mM) for 6 h, followed by treatment with recombinant mouse FGF21 (50 ng/ml) or vehicle for 24 h. (**A**,**B**) Immunoblot analysis for p-AMPK, total AMPK, phosphor-ACC, total ACC, PON1 after 24 h of FGF21 treatment. (**C**) Cellular ROS levels measured by DCFH-DA assay. (**D**) The mRNA expression levels of TGF-β, FN, and IL-6. (**E**) The activities of the MRC complex measured 24 h after treatment. Data are presented as mean ± S.E.M. **P*<0.05, ***P*<0.01; *n*=6–7 in each group. All *in vitro* data were obtained from at least four independent experiments.

its ability to hydrolyze and therefore detoxify organophosphorus compounds, which are widely used as pesticides and nerve gases. Due to its ability to destroy oxidized lipids, PON1 appears to play a role in some certain diseases. Recently, a number of studies have indicated that PON1 presents multiple biofunctions including anti-inflammatory, antioxidative, anti-atherogenic, antidiabetic, antimicrobial, and organophosphate-hydrolyzing properties. Therefore, it was considered as a potential agent against cardiovascular diseases due to these biocharacteristics [43]. In the present study, we first found that PON1 is involved in the pathogenesis of DCM. Cardiac PON1 is significantly decreased in STZ/HFD-induced WT diabetic mice followed by an increase in cardiac ROS production and a decrease in MRC complex activities, and the magnitude of decrease in PON1 content is further augmented in STZ/HFD-induced FGF21-deficient mice. In contrast, overexpression of FGF21 dramatically increases cardiac PON1 expression accompanied by a reduction in ROS level and inhibition of decreased MRC complex activities. Our *in vitro* data also indicate that the protective effects of FGF21 against HG-induced cytotoxicity are also strongly abrogated by inhibition

of PON1 in primary mouse cardiomyocytes, suggesting that the protective effects of FGF21 against diabetes-induced cardiac damage are at least in part mediated by the antioxidative effect of PON1.

AMPK is a serine-threonine kinase that acts as an energy sensor in various cellular types. AMPK acts as a metabolic master switch regulating several intracellular systems including the cellular uptake of glucose, the β-oxidation of fatty acids, and the biogenesis of glucose transporter 4 and mitochondria [44,45]. The energy-sensing capability of AMPK can be attributed to its ability to detect and react to fluctuations in the AMP:ATP ratio that take place during rest and exercise [45,46]. AMPK signaling pathways are activated by adipokines, including adiponectin and leptin secreted from adipose tissues, which play several distinct but important physiological and pathological roles in the body [47,48]. AMPK is significantly activated in response to cardiac energy imbalance during myocardial ischemia and myocardial infarction, and inactivation of AMPK was found to enhance myocardial injury during ischemia–reperfusion in mice [32,49]. Recently, we indicated that FGF21 protects against cardiac apoptosis in a type 1 diabetic mouse model by activating the extracellular signal-regulated kinase (ERK) 1/2-p38 mitogen-activated protein kinase (MAPK)-AMPK pathway [19], and pharmaceutical inhibition of AMPK led to a significant decrease in FGF21-induced cardioprotection and restoration of cardiac function in response to global ischemia [12]. In the present study, our *in vivo* data indicate that cardiac activation of AMPK was markedly up-regulated in STZ/HFD-induced diabetic mice. However, this elevation of AMPK activation was strongly attenuated in FGF21 KO mice, suggesting that FGF21 may be involved in the regulation of AMPK activity in response to restoring cardiac-energy homeostasis in STZ/HFD-induced diabetic mice. On the other hand, FGF21 inhibits palmitate-induced down-regulation of AMPK activation in cultured cardiomyocytes [19]. Consistent with these reports, our *in vitro* results also demonstrated that treatment with FGF21 significantly improved the activation of AMPK in response to HG-induced cytotoxicity in primary cardiomyocytes, and genetic inhibition of AMPK signaling markedly abrogated the protective effect of FGF21, suggesting that AMPK plays an indispensable role in FGF21 protection against HG-induced cardiomyocyte injury.

In summary, our present study demonstrates that FGF21 protection against DCM is mediated by activation of the AMPK signaling pathway and enhanced PON1 expression, which, in turn, inhibits HG-induced oxidative stress and leads to alleviation of local inflammation, fibrosis, and cardiomyocyte apoptosis, thereby protecting against DCM (Supplemental Figure S5). Further studies on large humanoid animals and clinical investigations are warranted to validate these findings in rodent models.

Clinical perspectives

- FGF21 is a metabolic hormone with pleiotropic effects on glucose metabolism and insulin sensitivity.
- In the present study, our data indicate that FGF21 protecting against DCM is mediated at least in part by activating AMPK-PON1 axis.
- Our findings enrich our knowledge on FGF21 and metabolic regulation, and reignite hope for the future development of effective antidiabetic complication therapies.

Acknowledgements

We thank Dr Ying Zhi and Dr Dewei Ye for their technical support related to the examination of heart function and the construction of the AAV-FGF21 virus system.

Funding

This work was supported by the National Natural Science Foundation of China General Program [grant number 81471075]; and the National Natural Science Foundation of China Major Program [grant number 91439123].

Competing interests

The authors declare that there are no competing interests associated with the manuscript.

Clinical Science (2017) **131** 1877–1893
DOI: 10.1042/CS20170271

Author contribution

F.W., B.W., S.Z., L.S., and X.P. researched the data. L.S., R.X., and Y.W. wrote the manuscript and researched the data. Y.W. and F.G. reviewed/edited the figures. X.L. and Z.L. contributed to the discussion and reviewed/edited the manuscript.

Abbreviations

AAV, adeno-associated virus; ACC, acetyl-CoA carboxylase; AMPK, AMP-activated protein kinase; ANG, angiotensinogen; ANP, atrial natriuretic peptide; Col-1, collagen-1; DCM, diabetic cardiomyopathy; DHE, dihydroethidium; DN, dominant-negative; ECHO, echocardiography; FGF21, fibroblast growth factor 21; FN, fibronectin; HFD, high-fat diet; HG, high glucose; H&E, hematoxylin-eosin; IL-6, interleukin-6; MCP-1, monocyte chemoattractant protein 1; MRC, mitochondrial respiratory chain; PON1, paraoxonase 1; rmFGF21, recombinant mouse fibroblast growth factor 21; ROS, reactive oxygen species; STZ, streptozotocin; TGF-β, transforming growth factor β; TNF-α, tumor necrosis factor α; α-SMA, α-smooth muscle actin.

References

1 Palomer, X., Salvado, L., Barroso, E. and Vazquez-Carrera, M. (2013) An overview of the crosstalk between inflammatory processes and metabolic dysregulation during diabetic cardiomyopathy. *Int. J. Cardiol.* **168**, 3160–3172
2 Guleria, R.S., Singh, A.B., Nizamutdinova, I.T., Souslova, T., Mohammad, A.A., Kendall, Jr, A. et al. (2013) Activation of retinoid receptor-mediated signaling ameliorates diabetes-induced cardiac dysfunction in Zucker diabetic rats. *J. Mol. Cell Cardiol.* **57**, 106–118
3 Fang, Z.Y., Prins, J.B. and Marvick, T.H. (2004) Diabetic cardiomyopathy: evidence, mechanisms, and therapeutic implications. *Endocr. Rev.* **25**, 543–567
4 Fukumoto, S. (2008) Actions and mode of actions of FGF19 subfamily members. *Endocr. J.* **55**, 23–31
5 Kharitonenkov, A. and Shanafelt, A.B. (2008) Fibroblast growth factor-21 as a therapeutic agent for metabolic diseases. *BioDrugs* **22**, 37–44
6 Kharitonenkov, A., Shiyanova, T.L., Koester, A., Ford, A.M., Micanovic, R., Galbreath, E.J. et al. (2005) FGF-21 as a novel metabolic regulator. *J. Clin. Invest.* **115**, 1627–35
7 Reitman, M.L. (2007) FGF21: a missing link in the biology of fasting. *Cell Metab.* **5**, 405–407
8 Lin, Z., Wu, Z., Yin, X., Liu, Y., Yan, X., Lin, S. et al. (2010) Serum levels of FGF-21 are increased in coronary heart disease patients and are independently associated with adverse lipid profile. *PLoS ONE* **5**, e15534
9 Zhang, W., Chu, S., Ding, W. and Wang, F. (2015) Serum level of fibroblast growth factor 21 is independently associated with acute myocardial infarction. *PLoS ONE* **10**, e0129791
10 Joki, Y., Ohashi, K., Yuasa, D., Shibata, R., Ito, M., Matsuo, K. et al. (2015) FGF21 attenuates pathological myocardial remodeling following myocardial infarction through the adiponectin-dependent mechanism. *Biochem. Biophys. Res. Commun.* **459**, 124–130
11 Lin, Z., Pan, X., Wu, F., Ye, D., Zhang, Y., Wang, Y. et al. (2015) Fibroblast growth factor 21 prevents atherosclerosis by suppression of hepatic sterol regulatory element-binding protein-2 and induction of adiponectin in mice. *Circulation* **131**, 1861–1871
12 Cong, W.T., Ling, J., Tian, H.S., Ling, R., Wang, Y., Huang, B.B. et al. (2013) Proteomic study on the protective mechanism of fibroblast growth factor 21 to ischemia-reperfusion injury. *Can. J. Physiol. Pharmacol.* **91**, 973–984
13 Liu, S.Q., Roberts, D., Kharitonenkov, A., Zhang, B., Hanson, S.M., Li, Y.C. et al. (2013) Endocrine protection of ischemic myocardium by FGF21 from the liver and adipose tissue. *Sci. Rep.* **3**, 2767
14 Planavila, A., Redondo, I., Hondares, E., Vinciguerra, M., Munts, C., Iglesias, R. et al. (2013) Fibroblast growth factor 21 protects against cardiac hypertrophy in mice. *Nat. Commun.* **4**, 2019
15 Yan, X., Chen, J., Zhang, C., Zhou, S., Zhang, Z., Chen, J. et al. (2015) FGF21 deletion exacerbates diabetic cardiomyopathy by aggravating cardiac lipid accumulation. *J. Cell. Mol. Med.* **19**, 1557–1568
16 Hotta, Y., Nakamura, H., Konishi, M., Murata, Y., Takagi, H., Matsumura, S. et al. (2009) Fibroblast growth factor 21 regulates lipolysis in white adipose tissue but is not required for ketogenesis and triglyceride clearance in liver. *Endocrinology* **150**, 4625–4633
17 Zhang, Z., Wang, S., Zhou, S., Yan, X., Wang, Y., Chen, J. et al. (2014) Sulforaphane prevents the development of cardiomyopathy in type 2 diabetic mice probably by reversing oxidative stress-induced inhibition of LKB1/AMPK pathway. *J. Mol. Cell Cardiol.* **77**, 42–52
18 Lin, Z., Tian, H., Lam, K.S., Lin, S., Hoo, R.S., Konishi, M. et al. (2013) Adiponectin mediates the metabolic effects of FGF21 on glucose homeostasis and insulin sensitivity in mice. *Cell Metab.* **17**, 779–789
19 Zhang, C., Huang, Z., Gu, J., Yan, X., Lu, X., Zhou, S. et al. (2015) Fibroblast growth factor 21 protects the heart from apoptosis in a diabetic mouse model via extracellular signal-regulated kinase 1/2-dependent signalling pathway. *Diabetologia* **58**, 1937–1948
20 Basu, R., Oudit, G.Y., Wang, X., Zhang, L., Ussher, J.R., Lopaschuk, G.D. et al. (2009) Type 1 diabetic cardiomyopathy in the Akita (Ins2WT/C96Y) mouse model is characterized by lipotoxicity and diastolic dysfunction with preserved systolic function. *Am. J. Physiol. Heart Circ. Physiol.* **297**, H2096–H2108
21 Abdalla, M.Y., Mathahs, M.M. and Ahmad, I.M. (2012) Reduced heme oxygenase-1 expression in steatotic livers infected with hepatitis C virus. *Eur. J. Intern. Med.* **23**, 649–655
22 Aviram, M., Hardak, E., Vaya, J., Mahmood, S., Milo, S., Hoffman, A. et al. (2000) Human serum paraoxonases (PON1) Q and R selectively decrease lipid peroxides in human coronary and carotid atherosclerotic lesions: PON1 esterase and peroxidase-like activities. *Circulation* **101**, 2510–2517
23 Tang, W.H., Hartiala, J., Fan, Y., Wu, Y., Stewart, A.F., Erdmann, J. et al. (2012) Clinical and genetic association of serum paraoxonase and arylesterase activities with cardiovascular risk. *Arterioscler. Thromb. Vasc. Biol.* **32**, 2803–2812

24 Lin, Z.F., Li, X.K., Lin, Y., Wu, F., Liang, L.M., Fu, X.B. et al. (2005) Protective effects of non-mitogenic human acidic fibroblast growth factor on hydrogen peroxide-induced damage to cardiomyocytes *in vitro*. *World J. Gastroenterol.* **11**, 5492–5497
25 Chang, J., Li, Y., Huang, Y., Lam, K.S., Hoo, R.L., Wong, W.T. et al. (2010) Adiponectin prevents diabetic premature senescence of endothelial progenitor cells and promotes endothelial repair by suppressing the p38 MAP kinase/p16INK4A signaling pathway. *Diabetes* **59**, 2949–2959
26 Cheng, K.K., Lam, K.S., Wang, Y. , Huang, Y., Carling, D., Wu, D. et al. (2007) Adiponectin-induced endothelial nitric oxide synthase activation and nitric oxide production are mediated by APPL1 in endothelial cells. *Diabetes* **56**, 1387–1394
27 Zhou, M., Xu, A., Tam, P.K., Lam, K.S., Chan, L., Hoo, R.L. et al. (2008) Mitochondrial dysfunction contributes to the increased vulnerabilities of adiponectin knockout mice to liver injury. *Hepatology* **48**, 1087–1096
28 Lin, Z., Wu, F., Lin, S., Pan, X., Jin, L., Lu, T. et al. (2014) Adiponectin protects against acetaminophen-induced mitochondrial dysfunction and acute liver injury by promoting autophagy in mice. *J. Hepatol.* **61**, 825–831
29 Ni, R., Cao, T., Xiong, S., Ma, J., Fan, G.C., Lacefield, J.C. et al. (2016) Therapeutic inhibition of mitochondrial reactive oxygen species with mito-TEMPO reduces diabetic cardiomyopathy. *Free Radic. Biol. Med.* **90**, 12–23
30 Schrauwen-Hinderling, V.B., Kooi, M.E. and Schrauwen, P. (2016) Mitochondrial function and diabetes: consequences for skeletal and cardiac muscle metabolism. *Antioxid. Redox Signal.* **24**, 39–51
31 Dingx, X., Boney-Montoya, J., Owen, B.M., Bookout, A.L., Coate, K.C., Mangelsdorf, D.J. et al. (2012) βKlotho is required for fibroblast growth factor 21 effects on growth and metabolism. *Cell Metab.* **16**, 387–393
32 Beauloye, C., Bertrand, L., Horman, S. and Hue, L. (2011) AMPK activation, a preventive therapeutic target in the transition from cardiac injury to heart failure. *Cardiovasc. Res.* **90**, 224–233
33 Zaha, V.G. et al. (2016) AMPK is critical for mitochondrial function during reperfusion after myocardial ischemia. *J. Mol. Cell Cardiol.* **91**, 104–113
34 Lee, S.Y., Ku, H.C., Kuo, Y.H., Chiu, H.L. and Su, M.J. (2015) Pyrrolidinyl caffeamide against ischemia/reperfusion injury in cardiomyocytes through AMPK/AKT pathways. *J. Biomed. Sci.* **22**, 18
35 She, Z.G., Zheng, W., Wei, Y.S., Chen, H.Z., Wang, A.B., Li, H.L. et al. (2009) Human paraoxonase gene cluster transgenic overexpression represses atherogenesis and promotes atherosclerotic plaque stability in ApoE-null mice. *Circ. Res.* **104**, 1160–1168
36 Ng, D.S., Chu, T., Esposito, B., Hui, P., Connelly, P. and Gross, P.L. (2008) Paraoxonase-1 deficiency in mice predisposes to vascular inflammation, oxidative stress, and thrombogenicity in the absence of hyperlipidemia. *Cardiovasc. Pathol.* **17**, 226–232
37 Guns, P.J., Van Assche, T., Verreth, W., Fransen, P., Mackness, B., Mackness, M. et al. (2008) Paraoxonase 1 gene transfer lowers vascular oxidative stress and improves vasomotor function in apolipoprotein E-deficient mice with pre-existing atherosclerosis. *Br. J. Pharmacol.* **153**, 508–16
38 Kharitonenkov, A., Wroblewski, V.J., Koester, A., Chen, Y.F., Clutinger, C.K., Tigno, X.T. et al. (2007) The metabolic state of diabetic monkeys is regulated by fibroblast growth factor-21. *Endocrinology* **148**, 774–781
39 Chau, M.D., Gao, J., Yang, Q., Wu, Z. and Gromada, J. (2010) Fibroblast growth factor 21 regulates energy metabolism by activating the AMPK-SIRT1-PGC-1alpha pathway. *Proc. Natl. Acad. Sci. U.S.A.* **107**, 12553–12558
40 Kuro-o, M., Matsumura, Y., Aizawa, H., Kawaguchi, H., Suga, T., Utsugi, T. et al. (1997) Mutation of the mouse klotho gene leads to a syndrome resembling ageing. *Nature* **390**, 45–51
41 Ogawa, Y., Kurosu, H., Yamamoto, M., Nandi, A., Rosenblatt, K.P., Goetz, R. et al. (2007) BetaKlotho is required for metabolic activity of fibroblast growth factor 21. *Proc. Natl. Acad. Sci. U.S.A.* **104**, 7432–7437
42 So, W.Y., Cheng, Q., Chen, L., Evans-Molina, C., Xu, A., Lam, K.S. et al. (2013) High glucose represses beta-klotho expression and impairs fibroblast growth factor 21 action in mouse pancreatic islets: involvement of peroxisome proliferator-activated receptor gamma signaling. *Diabetes* **62**, 3751–9
43 Mackness, M.I., Durrington, P.N. and Mackness, B. (2004) The role of paraoxonase 1 activity in cardiovascular disease: potential for therapeutic intervention. *Am. J. Cardiovasc. Drugs* **4**, 211–217
44 Ojuka, EO. (2004) Role of calcium and AMP kinase in the regulation of mitochondrial biogenesis and GLUT4 levels in muscle. *Proc. Nutr. Soc.* **63**, 275–278
45 Winder, W.W. and Thomson, D.M. (2007) Cellular energy sensing and signaling by AMP-activated protein kinase. *Cell Biochem. Biophys.* **47**, 332–347
46 Thomson, D.M., Porter, B.B., Tall, J.H., Kim, H.J., Barrow, J.R. and Winder, W.W. (2007) Skeletal muscle and heart LKB1 deficiency causes decreased voluntary running and reduced muscle mitochondrial marker enzyme expression in mice. *Am. J. Physiol. Endocrinol. Metab.* **292**, E196–E202
47 Minokoshi, Y., Kim, Y.B., Peroni, O.D., Fryer, L.G., Muller, C., Carling, D. et al. (2002) Leptin stimulates fatty-acid oxidation by activating AMP-activated protein kinase. *Nature* **415**, 339–343
48 Yamauchi, T., Kamon, J., Minokoshi, Y., Ito, Y., Waki, H., Uchida, S. et al. (2002) Adiponectin stimulates glucose utilization and fatty-acid oxidation by activating AMP-activated protein kinase. *Nat. Med.* **8**, 1288–1295
49 Morrison, A. and Li, J. (2011) PPAR-gamma and AMPK–advantageous targets for myocardial ischemia/reperfusion therapy. *Biochem. Pharmacol.* **82**, 195–200